IOPscience iopscience.iop.org

Home Search Collections Journals About Contact us My IOPscience

Strongly coupled polyelectrolyte–macroion complexes

This article has been downloaded from IOPscience. Please scroll down to see the full text article.

2005 J. Phys.: Condens. Matter 17 S1137

(http://iopscience.iop.org/0953-8984/17/14/002)

View the table of contents for this issue, or go to the journal homepage for more

Download details:
IP Address: 129.252.86.83
The article was downloaded on 27/05/2010 at 20:35

Please note that terms and conditions apply.

INSTITUTE OF PHYSICS PUBLISHING JOURNAL OF PHYSICS: CONDENSED MATTER

J. Phys.: Condens. Matter **17** (2005) S1137–S1151 doi:10.1088/0953-8984/17/14/002

Strongly coupled polyelectrolyte–macroion complexes

Hoda Boroudjerdi and Roland R Netz

Physics Department, Technical University Munich, James Franck Street, D-85748 Garching, Germany

Received 22 October 2004, in final form 23 December 2004
Published 24 March 2005
Online at stacks.iop.org/JPhysCM/17/S1137

Abstract

We review the problem of complex formation between a macroion and an oppositely charged polyelectrolyte on the linear level. We study the effect of changing the ionic strength and the valency of the macroion on the complexed polymer configuration. Distinguishing four different configurational symmetry classes, we are able to map out the global configurational phase diagram. We also study the interaction between two complexes of macroion and polyelectrolyte, which gives rise to configurational changes of two complexes as they approach each other. Most of these calculations are performed on the ground-state level and are thus accurate only for very stiff polymers or highly charged and therefore strongly bound systems. We also give a short outlook into the problem of thermal fluctuations around the polymer ground state configuration as it is wrapped around the macroion. This problem is tackled by a normal-mode analysis. All calculations are performed for parameters corresponding to DNA–histone complexes, which are the basic building blocks of the nucleosomal genetic structure.

(Some figures in this article are in colour only in the electronic version)

1. Introduction

Complexes formed between polyelectrolytes and oppositely charged macroions have attracted much attention recently due to their vast technological applications. Examples are furnished by the complexation of synthetic polyelectrolytes with charged micelles [1, 2], charged plastic beads [3], gold particles [4, 5], or dendrimers [6]. Polyelectrolyte–macroion complexes are also important from a fundamental point of view as they are connected closely with several other interesting problems such as like-charge attraction due to structural correlations [7–9] and overcharging of a macroion with oppositely charged polymers [10] which can trigger charge-oscillating multilayer adsorption [11, 12]. But perhaps the most striking example of polyelectrolyte–macroion complexation occurs in the packaging process of DNA in the nucleus of the cell, in which a total length of about 1 m of DNA—with a total negative charge of $10^{10}e$ (i.e. one elementary charge, e, per 1.7 Å)—is stored inside the cell nucleus

 © 2005 IOP Publishing Ltd Printed in the UK

of few micrometres in diameter [13–19]. The DNA packaging process involves a hierarchical structure, on the lowest level of which DNA is wrapped twice around positively charged proteins called histones, which forms the structure known as the nucleosome. In the chromatin structure, these nucleosomes are arrayed like beads on a string and form various types of higher order structures [13–22].

The nucleosome structure has been studied widely *in vitro*, since the linker DNA (a piece of DNA connecting two nucleosomes in chromatin) can be cut by nuclease digestion process [14, 20] giving single nucleosomes. Further digestion of any eukaryotic cell's chromatin will lead to nucleosomal core particles (NCPs) consisting of a short segment of DNA with nearly 146 base pairs (and a length of about 50 nm) and a histone octamer of few nanometres in diameter (about 6 nm). Numerous *in vitro* experiments are done on NCPs aiming to obtain an understanding of what mechanisms may be involved *in vivo*. These experiments have addressed the DNA-adsorption process on histones [21, 23–25], interactions between NCPs [8, 9], and also the behaviour of NCPs under mechanical stress [26–28]. It is particularly known that surrounding conditions, such as pH and the ionic strength of the solution, affect the NCP structure. For instance, it has been shown experimentally [21] that the tightly wrapped state of DNA around the histone core is only stable for intermediate, physiological salt concentrations, at which an optimal balance between electrostatic self-repulsion of DNA segments and the DNA–histone electrostatic attraction is achieved.

The complexation of polyelectrolytes with macroions has also been investigated theoretically [3, 29–47] with particular attention paid to the DNA–histone system. The adsorption of rather flexible polyelectrolytes on charged spheres was studied using variational and self-consistent methods [3, 29–31], where the adsorbed chains form a rather homogeneous charge distribution and mean-field-like approximations can be used. A different approach [32–35] employs a ground-state analysis when the persistence length of chains is larger than the sphere radius. In this case, the polymer density distribution is rather inhomogeneous and the fluctuations around the optimal polymer configuration are weak if the adsorption energy is sufficiently large. Such studies exhibit a wrapping transition between a tightly wrapped state of the polymer and a state where the adsorption energy is not large enough to overcome the bending rigidity of the polymer. An interesting issue is the effective charge of a complex, as it was realized that macroions can indeed be overcharged, which occurs as more polyelectrolyte adsorbs on a charged sphere [34, 36–39] (or also on charged plates [48] and cylinders [49, 50]) than is necessary to neutralize the macroion charge. Overcharging can be obtained in the absence of salt ions and counterions in which case it is energetic in nature, driven by structural correlations [10, 36–38, 50]. It can also be obtained in the presence of salt on the linear (Debye–Hückel) level [34, 48, 50], though non-linear effects associated with counterion release dominate the behaviour for highly charged objects at low salt concentration [39, 49].

In the present paper, we review the complexation of a polyelectrolyte chain with a spherical macroion in a simplified model with parameters chosen appropriate for the DNA–histone system (though with some suitable rescaling the results can be applied to other systems as well). We consider both the case of no salt, where charges interact with bare Coulomb interaction, and also the case with added salt, for which electrostatic interactions are described within a linear approximation using the Debye–Hückel theory. Nonlinear effects associated with counterion condensation can be treated using a simple charge renormalization scheme due to Manning [51, 53]. As we shall see in section 2, the complexation behaviour of a single polyelectrolyte on a macroion can be classified within the ground-state analysis by considering symmetries of the polyelectrolyte configuration on the charged sphere. One can obtain the global phase diagram of this system using conveniently defined order parameters in terms of macroion charge and salt concentration [52, 53]. In section 3, we shall review the

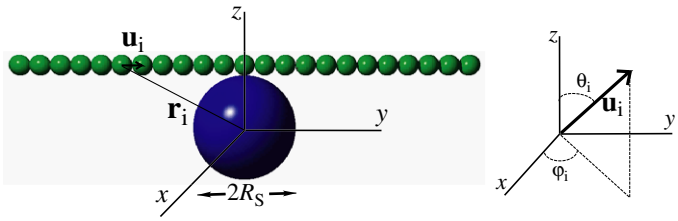

Figure 1. Schematic view of the discretized model. The macroion is modelled as a sphere with total charge of Z and the polyelectrolyte chain is modelled as a Kratky–Porod chain. The chain is discretized into subunits, $\mathbf{u}_i$, which have a fixed length and are characterized by their polar and azimuthal angles.

results of a similar analysis on the effective interaction between two such complexes (each of them consisting of a single chain and a charged sphere). Several configurational phases can be distinguished using symmetry arguments including a bridging phase (in which a polyelectrolyte bridges between the two complexes), and an asymmetric phase (in which complexes bind as a result of structural correlation induced by polymer configurational changes). In both phases, there is an effective short-range attraction between two effectively *like-charged* complexes, which are already overcharged by the polyelectrolyte chain. The effective attraction gives rise to a non-monotonic behaviour in the virial coefficient of the system, exhibiting a pronounced minimum at about the physiological salt concentration (100 mM monovalent salt), which compares well with experimental observations [8]. Finally, in section 4, some notes on chain fluctuations are added, which can be treated using a normal-mode approach for sufficiently stiff and strongly bound polymers.

2. Phase behaviour of a single polyelectrolyte–macroion complex

Let us consider a simplified model of complexation in which the polyelectrolyte (PE) is described by a semiflexible worm-like chain of length L and the macroion is modelled as a semi-rigid, impenetrable sphere of radius R_s (see figure 1). The polyelectrolyte chain is assumed to have a linear charge density of $-\tau$ and a persistence length of ℓ_p, and the oppositely charged sphere has a total charge of Z (both τ and Z are given in units of the elementary charge e and are positive by definition).

The electrostatic interaction between the PE chain and the spherical macroion is taken into account using the Debye–Hückel (DH) potential, which considers co- and counterions implicitly, and thus neglects nonlinear effects associated with counterions. These effects can be systematically included within the nonlinear Poisson–Boltzmann (PB) theory [54]. However, obtaining the optimal PE configuration using the full PB theory is at present numerically not achievable, and other, more approximate, methods have to be used to capture such nonlinear effects [53] (see below). We shall also neglect hydrogen bonds, van der Waals forces and the solvent structure within the present description (the solvent is treated as a continuum dielectric medium of uniform dielectric constant $\varepsilon = 80$, being equal to that of water at room temperature). Excluded-volume interactions act between the chain monomers and the sphere by assuming a short-range soft-core repulsion adjusted such that the impenetrability of the sphere is guaranteed.

The effective Hamiltonian of this model may be written as the combination of two terms

$$\mathcal{F} = \mathcal{F}_p + \mathcal{F}_{pm}, \tag{1}$$

in which

$$\frac{\mathcal{F}_{\rm p}}{k_{\rm B}T} = \frac{\ell_{\rm p}}{2}\int_0^L {\rm d}s\, \ddot{\mathbf{r}}^2(s) + \tau^2 \ell_{\rm B}\int_0^L {\rm d}s \int_s^L {\rm d}s' \, \frac{{\rm e}^{-\kappa|\mathbf{r}(s)-\mathbf{r}(s')|}}{|\mathbf{r}(s)-\mathbf{r}(s')|} \tag{2}$$

is the self-energy of the chain comprising mechanical bending rigidity (the first term) and electrostatic self-energy (the second term) in units of $k_{\rm B}T$. Here $\mathbf{r}(s)$ specifies the configuration of the chain with s being the contour parameter. The other contribution comes from the PE–macroion interaction energy, that is

$$\frac{\mathcal{F}_{\rm pm}}{k_{\rm B}T} = -\frac{\ell_{\rm B} Z\tau {\rm e}^{\kappa R_{\rm s}}}{1+\kappa R_{\rm s}}\int_0^L {\rm d}s\, \frac{{\rm e}^{-\kappa|\mathbf{r}(s)|}}{|\mathbf{r}(s)|} + \frac{ZA{\rm e}^{R_{\rm s}/\alpha}}{1+\kappa R_{\rm s}}\int_0^L {\rm d}s\, {\rm e}^{-|\mathbf{r}(s)|/\alpha}, \tag{3}$$

where the first term is the electrostatic contribution and the second term represents the soft-core repulsion term characterized by two parameters A and α for the strength and the range of repulsion respectively[1]. Taking a soft potential is crucial when investigating thermal fluctuations of the PE chain adsorbed on the sphere—see section 4.

In the above equations, $\ell_{\rm B} = e^2/(4\pi\varepsilon\varepsilon_0 k_{\rm B}T)$ is the so-called Bjerrum length, which gives a measure of the strength of electrostatic interactions compared to the thermal energy (in water and at room temperature $\ell_{\rm B} \approx 0.7$ nm). Another important parameter is the Debye screening length, which is given by κ^{-1}, where $\kappa^2 = 8\pi\ell_{\rm B} I$ with $I = \frac{1}{2}\sum_i z_i^2 c_i$ representing the ionic strength in the presence of a mixture of salt ion species (of charge valency z_i and concentration c_i for the species i). The self-energy terms (both mechanical and electrostatic) tend to straighten the chain, while the chain–sphere attraction tends to bend the chain and thus favours the complexation. As we shall see in the following sections, the competition between these factors leads to different configurational phases depending on the salt concentration (entering via κ) and macroion charge, Z. These two parameters are chosen as the main phase variables reflecting their important role in experiments, where various phases are revealed by changing the salt concentration [21]. The effective charge of histones may also vary depending on the surrounding conditions, such as pH of the solution, which affects the ionization of proteins. Hence treating Z as an independent variable allows us to cover a variety of different experimental regimes.

In the following we choose parameter values suitable for DNA–histone complexes, i.e. $L = 49.64$ nm corresponding to 146 base pairs of DNA, $\ell_{\rm p} = 30$ nm as the bare mechanical persistence length of DNA, and $R_{\rm s} = 5$ nm as the effective histone radius (which also includes the radius of DNA and thus corresponds to the distance of closest approach), and $\tau = 5.88\ {\rm nm}^{-1}$. This linear charge density corresponds to the maximum dissociation of phosphate groups in the case of DNA giving rise to a charge of $2e$ per base pair (of 0.34 nm length). Note that in reality the actual charge may be reduced from its bare value due to counterion condensation and charge regulation processes, though for a short chain of uniform charge density as considered above such effects are expected to be weak (condensation of counterions is further suppressed due to the presence of the charged sphere). Nonetheless, one can account for counterion condensation effects within the Debye–Hückel scheme using Manning condensation theory for an isolated long polymer [51], which implies a reduced linear charge density of $\tau_{\rm M} = 1/\ell_{\rm B} \approx 1.4\ {\rm nm}^{-1}$ for monovalent counterions. This gives the lower limit for the charge density of a linear chain. Yet, as shown in [53], the phase behaviour of the system remains qualitatively unchanged in the presence of counterion condensation. We shall not discuss these effects further in this paper and also assume that salt ions are monovalent

[1] Note that α, which gives a measure of the 'softness' of the sphere, should be taken smaller than κ^{-1}, so that the beads are allowed to reside near the sphere [55]. Also, the prefactor of the soft-core repulsion is chosen to be proportional to the strength of the electrostatic attraction and thus contains the effective charge of the sphere $Z/(1+\kappa R_{\rm s})$.

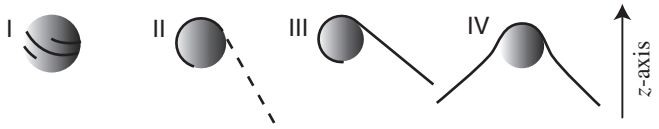

Figure 2. Schematic view of four different symmetry states characterized by the two independent symmetries of twofold rotational symmetry and mirror reflection [53].

($z_i = \pm 1$), since for large charge valency electrostatic correlations due to counterions become important and the present model breaks down.

2.1. Ground-state analysis

In analysing the above model for the DNA–histone complex, we take advantage of the short length of the chain ($L \approx 50$ nm) compared with its persistence length (which is at least $\ell_p = 30$ nm for DNA, even without additional chain stiffening due to electrostatic repulsions). We can therefore neglect the fluctuations of the chain and employ a ground-state analysis [34] where one has to determine the optimal chain configuration at the macroion, which minimizes the effective Hamiltonian in equation (1) (with the condition of no stretching, $|\dot{\mathbf{r}}(s)| = 1$). The minimization procedure is difficult to perform analytically in three dimensions [34], while numerical minimization methods prove quite successful in determining the optimal chain conformation in a wide range of system parameters. The goal is achieved by discretizing the chain using N rigid subunits, where the subunits have no relation with physical monomers of the PE chain. Each subunit, which has a fixed length, is characterized by a vector (and thus two polar and azimuthal angles θ_i and ϕ_i) and the minimization is performed in the configuration space of all subunit angles [53]—see figure 1.

It turns out that different (ground-state) conformations of the PE chain at the charged sphere may be classified into four different (configurational) phases, which are distinguished by geometric symmetries of the chain configuration [52, 53]. These phases are shown schematically in figure 2 and are referred to as phases I, II, III and IV. (The numerically obtained conformations of the chain are shown in figure 3.) In phase I, the complex exhibits a *twofold rotational* symmetry about the axis which connects the midpoint of the chain and the sphere centre, and occurs only when the PE chain is totally wrapped around the sphere. Phase II corresponds to an asymmetric three-dimensional configuration of the chain. In phase III, the chain has a two-dimensional (planar) geometry and possesses only the *mirror* symmetry. In phase IV, the chain has both rotational and mirror symmetries mentioned above, and represents a fully symmetric state. Each of these phases is obtained in a certain range of salt concentration and sphere charge (see below).

In figure 3, the evolution of chain conformations is shown for $Z = 40$ and increasing salt concentration. As seen, in the absence of salt ($\kappa = 0$), the fully symmetric phase IV is obtained, where the chain shows an unwrapped configuration. In this case, the electrostatic self-energy of the chain (which results from unscreened repulsions of chain segments) is dominant compared with the chain–sphere attraction (see equations (1)–(3)). As the salt concentration increases ($\kappa = 0.08$ nm^{-1}), the chain configuration undergoes a transition to the partially wrapped phase III. For higher salt concentration ($\kappa = 0.14$ nm^{-1}), the asymmetric phase II is obtained as the optimal state of the chain, where the chain is again partially wrapped but has a three-dimensional structure as mentioned above. Note that the electrostatic self-repulsion of the chain becomes weaker as κ increases, and at intermediate salt concentrations ($\kappa = 0.418$ nm^{-1}) the chain becomes completely wrapped around the sphere (phase I). Further increase of the

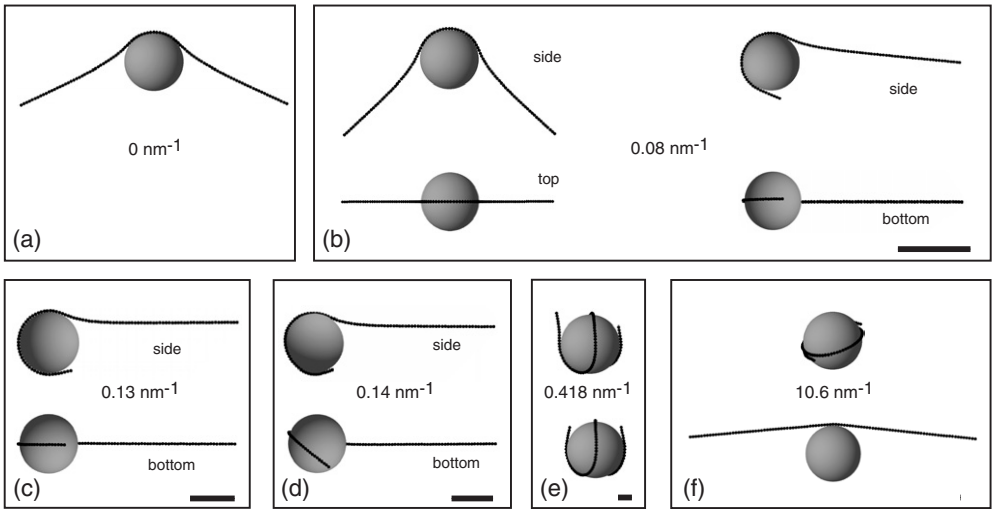

Figure 3. Various configurations for the chain–sphere complex as obtained by numerical minimization of equation (1) for fixed sphere charge $Z = 40$ and several salt concentrations (bars on lower right indicate the respective screening length except when infinite): (a) At $\kappa = 0$ (no added salt), the configuration shows rotational and mirror symmetry (unwrapped state). (b) At $\kappa = 0.08$ nm^{-1} the rotational symmetry is broken and both the structures shown coexist. The chain configuration is still mirror symmetric as demonstrated by the top and bottom view. (c) At $\kappa = 0.13$ nm^{-1}, the mirror symmetry is broken which is shown here right at the transition. (d) The mirror asymmetric configuration at a slightly elevated salt concentration $\kappa = 0.14$ nm^{-1}. (e) At $\kappa = 0.418$ nm^{-1}, the rotational symmetry is restored, as witnessed by the two coexisting structures which are rather similar. (f) Coexistence between fully wrapped and unwrapped configurations at $\kappa = 10.6$ nm^{-1}.

salt concentration leads to strong screening of electrostatic interactions, and eventually the mechanical bending rigidity dominates, leading to the unwrapped state of the chain (phase IV) for sufficiently large κ.

The transitions between these configurational phases are associated with symmetry-breaking (or restoring) processes, which may be continuous or discontinuous as can be determined by considering relevant order parameters (which reflect geometric symmetries of the chain conformation), and also from the behaviour of the energy at the transition points. We shall not discuss these aspects in detail here (see [52, 53] for more details), just note that at a discontinuous transition there is a coexistence between two different configurational phases. For instance, we show two such coexisting configurations for $Z = 40$ in figures 3(b), (e) and (f). In figure 3(e), two configurations from phase II (top) and phase I (bottom) are obtained as the optimal configurations with the same energy. In figure 3(f), a similar situation is obtained, where two configurations from phase I (top) and phase IV (bottom) coexist.

2.2. Global phase diagram

The complexation behaviour of the chain–sphere system may be summarized into a global phase diagram in terms of κ (inverse screening length) and Z (sphere charge) as shown in figure 4. (Figure 4(a) shows the phases in a wide range of κ up to 10 nm^{-1}, and figure 4(b) represents details of the phase diagram for small κ.) The wrapping transition is obtained for all ranges of κ, though at small salt concentration (small κ) this transition occurs for larger

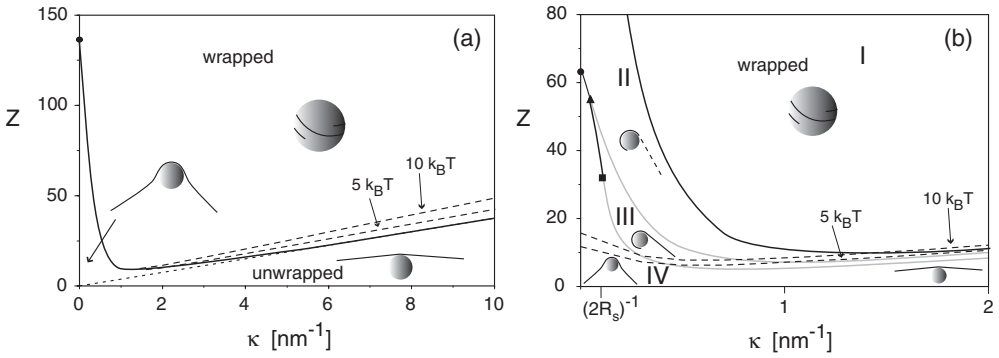

Figure 4. Phase diagram for the chain–sphere system as a function of the sphere charge Z and the inverse screening length κ. (a) The solid curve indicates the transition from the wrapped state (phase I) to the 3D asymmetric state (phase II). The dotted line is obtained from a local-energy-balance argument for this wrapping transition and is valid for large salt concentrations. (b) Details of the phase diagram for small κ, featuring all four different phases. Discontinuous (continuous) transitions are denoted by black (grey) solid curves [53]. The dashed curves in (a) and (b) indicate a complexation energy of $5k_BT$ and $10k_BT$.

values of sphere charge Z (in the absence of salt, $\kappa = 0$, the wrapping transition occurs at $Z = 133$). In agreement with experiments [21], complexation is more pronounced at intermediate salt concentrations. The minimal sphere charge to wrap the chain, $Z_* \approx 12$, is obtained for $\kappa^{-1} \approx 1$ nm (salt concentration $c_s \approx 0.1$ M for monovalent salt), which is close to physiological conditions. Since the total charge on the chain is about $-300e$ (using DNA parameters), the complex is strongly *overcharged* for all $Z < 300$, i.e. in the whole region of phase I shown in figure 4(a).

The dotted line in figure 4(a) is the high-salt prediction for the wrapping transition, which is obtained by locally balancing the various terms in the effective Hamiltonian, equation (1): namely the bending energy per unit length $\sim \ell_p/(2R_s^2)$, and the electrostatic attraction per unit length $\sim \ell_B Z\tau/\kappa R_s^2$ (in the limit of $\kappa R_s > 1$), leading to the line defined by $Z \approx \ell_p \kappa/2\ell_B\tau$ [34] (note that for large κ we can omit the electrostatic self-repulsion of the chain). This prediction (dotted line) agrees well with our numerical results for large salt concentration (solid curve) as can be seen in figure 4(a). The broken lines in figures 4(a) and (b) correspond to the constant complexation energy of $5k_BT$ and $10k_BT$, where the complexation energy is defined as the difference of the energy equation (1) in the ground state and the reference state consisting of a straight chain touching the sphere in the middle point (as for example shown in figure 1). It is seen that the complexation energy is much larger than k_BT except very close to high salt wrapping transition. This shows that thermal fluctuations can hardly result in unwrapping of the complex and can be omitted in the main part of the phase diagram [53].

Figure 4(b) shows the symmetry-breaking transitions in the low-κ region (grey curves show continuous transitions and black curves show discontinuous transitions [52, 53]). The bottom curve denotes the transition from the unwrapped phase IV to the 2D partially wrapped phase III, in which the twofold rotational symmetry is broken. The middle curve is the transition between phase III and the 3D asymmetric phase II, which is associated with the breaking of the mirror symmetry. At small κ and about $Z \approx 60$, there is a direct transition between phase II and the fully symmetric phase IV, which involves the breaking of both rotational and mirror symmetries. The upper curve in figure 4(b) is the same curve as in figure 4(a) representing the wrapping transition to phase I.

3. Two polyelectrolyte–macroion complexes

In the preceding section, we discussed the phase behaviour of a single isolated complex. But in order to understand the properties of complexes in solution, one has to consider the interaction between different complexes. These interactions are relevant at salt concentrations where the typical distance between complexes is smaller than the screening length. As shown in experiments on nucleosome core particles (NCPs) [8], the effective interaction between complexes can become attractive, which leads to a negative second virial coefficient. Though the underlying mechanism which yields attraction between two NCPs is not yet completely understood, we show that such attractive forces can result from an interplay between electrostatic contributions and configurational changes of the polyelectrolyte chain, which leads to structural correlations between two complexes at small distances [55].

Let us consider two polyelectrolyte–macroion complexes at a centre-to-centre distance of D from each other. We use the same model as described in section 2 for a single complex with the same parameters representing the DNA–histone system. We consider the effective interaction between the complexes and discuss the configurational changes of the chain for various values of the inverse screening length, κ, and sphere charge, Z, as a function of the distance between spheres, D.

The effective Hamiltonian of the two-complex system may be written as

$$\mathcal{F} = \sum_{\alpha=1,2} \mathcal{F}_{\mathrm{p}}[\mathbf{r}_\alpha] + \sum_{\alpha=1,2} \sum_{\beta=1,2} \mathcal{F}_{\mathrm{pm}}[\mathbf{r}_\alpha, \mathbf{R}_\beta] + \mathcal{F}_1 \tag{4}$$

where $\mathcal{F}_{\mathrm{p}}$ and $\mathcal{F}_{\mathrm{pm}}$ are given in equations (2) and (3). The first term in equation (4) represents the self-energy (electrostatic and mechanical bending) of chains in both complexes (labelled by $\alpha, \beta = 1, 2$) and the second term gives the interaction between the PE chains and the spheres ($\mathbf{r}_\alpha(s)$ specifies the configuration of the PE chain in complex α and $\mathbf{R}_\beta$ gives the position of the sphere centre in complex β). The third term contains the repulsion between the two PE chains and between the two spheres and reads

$$\frac{\mathcal{F}_1}{k_{\mathrm{B}}T} = \tau^2 \ell_{\mathrm{B}} \int_0^L \mathrm{d}s \int_0^L \mathrm{d}s' \, \frac{\mathrm{e}^{-\kappa|\mathbf{r}_1(s)-\mathbf{r}_2(s')|}}{|\mathbf{r}_1(s)-\mathbf{r}_2(s')|} + \frac{Z^2 \ell_{\mathrm{B}} \mathrm{e}^{2\kappa R_{\mathrm{s}}}}{(1+\kappa R_{\mathrm{s}})^2} \frac{\mathrm{e}^{-\kappa D}}{D} \tag{5}$$

where $D = |\mathbf{R}_1 - \mathbf{R}_2|$.

Similar to the calculation made for a single complex, we focus on the ground-state properties of this system. This approximation is expected to be valid for chain lengths not much longer than the persistence length (we use a chain length of $L \approx 50$ nm corresponding to 146 base pairs of DNA with bare persistence length of about 30 nm). We thus obtain the optimal configuration of the chains on both complexes from equation (4) for a given set of parameters by employing numerical minimization methods on a discretized model of the chains (compare section 2) [55].

3.1. Configurations and symmetries

In figure 5, we show a few ground-state configurations for fixed sphere charge ($Z = 100$) and fixed salt concentration (with inverse screening length $\kappa = 2\ \mathrm{nm}^{-1}$) for varying sphere–sphere distance. For large distances, the complexes exhibit the same chain configuration as in the case of a single isolated complex (section 2), since the surface separation between spheres is much larger than the screening length ($\kappa^{-1} = 0.5$ nm in the figure). At $D = 12.8$ nm the symmetry between the conformation of the chains on both spheres is broken, and for even smaller distances $D < 10.8$ nm a bridging conformation is found in which one PE is bound to both spheres. Note that at $D = 10.8$ nm the non-bridging and bridging states coexist,

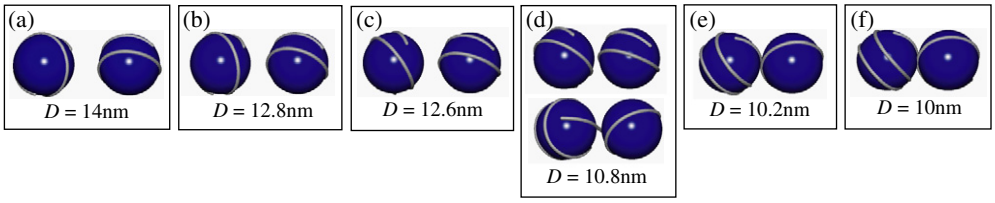

Figure 5. Ground-state configurations of the two-complex system for sphere charge $Z = 100$ and inverse screening length $\kappa = 2$ nm^{-1} for various sphere distances D. At $D = 12.8$ nm the symmetry between the two PEs is continuously broken and at $D = 10.8$ nm a discontinuous bridging transition takes place.

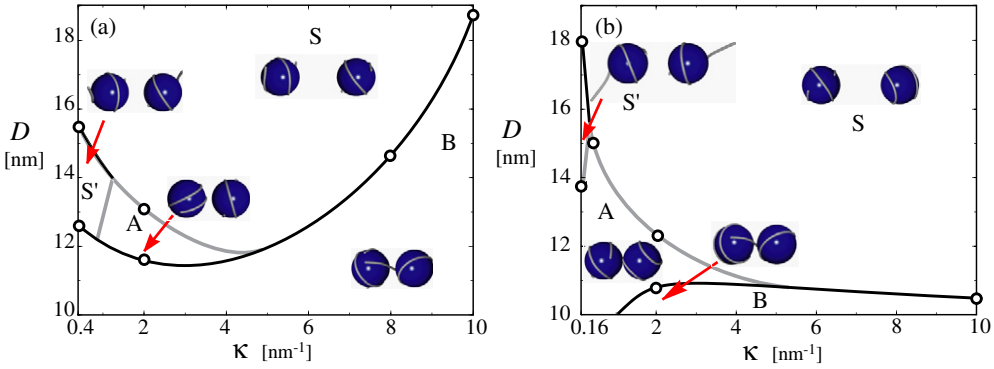

Figure 6. Phase diagram for two chain–sphere complexes as a function of the inverse Debye screening length κ and sphere centre-to-centre distance D for (a) sphere charge $Z = 40$ and (b) $Z = 100$, featuring symmetric (S, S′), asymmetric (A) and bridging phases (B). Black (grey) curves denote discontinuous (continuous) phase boundaries. Shown are actual configurations calculated in the respective phases.

i.e. they are both obtained as the optimal configuration of the system with the same energy. The configurational changes of the chains in fact indicate a series of configurational phase transitions, which can be characterized by considering suitable order parameters [55]. We distinguish a *symmetric phase*, denoted by S, where both complexes show the same structure, from an *asymmetric phase*, denoted by A, where due to mutual interactions the two complexes exhibit different structures. An extreme example of such symmetry breaking is the *bridging phase*, denoted by B, where one of the two chains is adsorbed simultaneously on both spheres.

We summarize various configurational phases of the two-complex system (on the ground-state level) in figure 6 for two values of the sphere charge $Z = 40$ (a) and $Z = 100$ (b). As intuitively expected at large sphere separations the symmetric phase S prevails. But at small separation the bridging phase B is stable. For very small salt concentration (i.e. for long-ranged Coulomb interaction), a second symmetric phase (S′) appears, in which the conformations of PE chains are similar, but each complex exhibits a configuration different from the isolated chain case with a large relative dipole moment (caused by extending PE tails). It is important to keep in mind that individual complexes are wrapped in the salt concentration range specified by $0.42\ \text{nm}^{-1} < \kappa < 10.0\ \text{nm}^{-1}$ ($0.16\ \text{nm}^{-1} < \kappa < 25.2\ \text{nm}^{-1}$) for $Z = 40$ ($Z = 100$).

The transitions between different phases may be continuous or discontinuous (as indicated in figure 6 with grey and black curves respectively), which appear as continuous or discontinuous changes in order parameters [55]. A discontinuous transition can also be identified from the

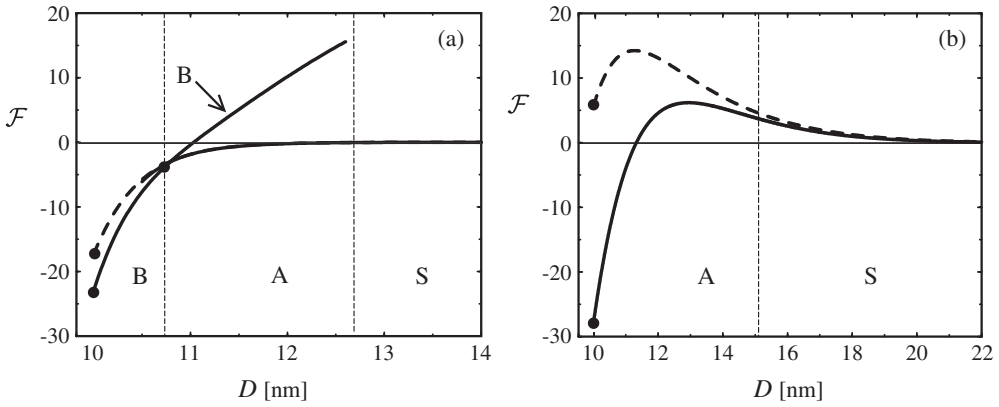

Figure 7. Energy of the two-complex system (in units of $k_B T$) within full optimization (solid curve) and constrained, rotational minimization [55] (broken curve) for $Z = 100$ and (a) $\kappa = 2$ nm^{-1} and (b) $\kappa = 0.40$ nm^{-1}. In (a) the transition between phases (B) and (A) at $D = 10.8$ nm is discontinuous, while the transition between phases (S) and (A) is continuous. In (b) the transition between the symmetric (S) and asymmetric (A) states is continuous.

effective Hamiltonian of the system, equation (4), which exhibits two stable minima reflecting the coexistence of two different structures. We present the energy of the system (solid curves) as a function of distance D for $Z = 100$ and for $\kappa = 2\,\text{nm}^{-1}$ and $\kappa = 0.40\,\text{nm}^{-1}$ in figures 7(a) and (b) respectively, where the reference state is taken at $D = \infty$. Figure 7(a) corresponds to configurations shown in figure 5. The discontinuous bridging transition at $D = 10.8$ nm is clearly identified by the crossing of the energy of the bridging and asymmetric phases. The bridging phase is stable for smaller separation and meta-stable for larger separation. The meta-stable solution of the asymmetric phase disappears at separations smaller than $D \approx 10.6$ nm.

3.2. Attractive interaction and the second virial coefficient

As already seen from the optimal configurations in figures 5 and 6, two chain–sphere complexes can become highly coupled at small separations in the bridging and asymmetric phases. In these regimes, PE chains on different spheres adapt their orientation and conformation in such a way that opposite charges from different complexes face each other. This reflects structural correlations between complexes at small distances, which emerge as a result of the inter-relation between electrostatic and bending contributions as the system obtains its optimal (ground-state) configuration. These effects lead to an effective *attraction* between two complexes at small distances as seen from the interaction energy curves in figure 7. Note that in this situation both complexes are highly overcharged (e.g. have a total negative charge of up to $200e$ for $Z = 100$ and DNA charge density $\tau = 5.88\,\text{nm}^{-1}$). The above result therefore resembles the attraction mechanism obtained for like-charged macroions in the strong-coupling limit, which arises from structural correlations at counterionic layers on opposite macroion surfaces [7, 10].

In figure 7, we also show the behaviour of the effective interaction energy obtained using *constrained optimization* (broken curves), where the chain configurations on the spheres are fixed to the ones in the isolated case ($D = \infty$), and only their orientation may vary. Note that both full optimization and constrained optimization lead to an attractive force, though only the former case gives a negative effective energy for $\kappa = 0.4\,\text{nm}^{-1}$ (figure 7(b)). The attraction within constrained optimization is only induced by changes in the orientation of chains and the bridging state is not present.

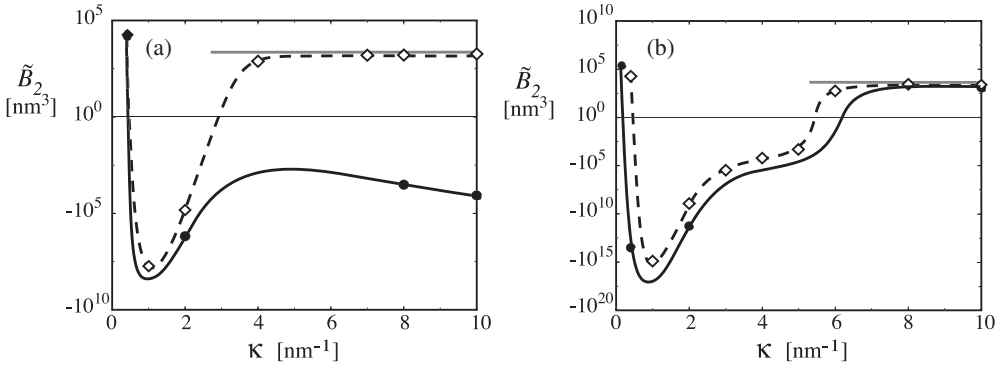

Figure 8. The rescaled second virial coefficient $\tilde{B}_2 = B_2(1 + |B_2|)/|B_2|$ as a function of κ (a) for $Z = 40$, (b) for $Z = 100$. Shown are results for the full optimization (solid curves) and rotational constrained optimization (broken curves). The horizontal grey lines denote the hard-core limit.

In the final step, we calculate the second virial coefficient B_2 associated with PE–macroion complexes, which is defined as

$$B_2 = \tfrac{2}{3}\pi(2R_s)^3 + 2\pi \int_{2R_s}^{\infty} \mathrm{d}D\, D^2(1 - \mathrm{e}^{-\mathcal{F}(D)}), \tag{6}$$

where the first term represents the hard-core (ideal) contribution and the second term takes into account the effective interaction between complexes, $\mathcal{F}(D)$ (in units of k_BT), which is obtained by numerical optimization of the chain configuration at a given D as discussed before. The connection with the osmotic pressure P of a nucleosomal-particle solution of concentration c is furnished by the relation

$$\frac{P}{k_BT} = c + B_2c^2 + \mathcal{O}(c^3). \tag{7}$$

In the limit of large salt concentration, the electrostatic contribution disappears and B_2 tends to the purely hard-core result. On the other hand, for vanishing salt concentration, the integral in equation (6) diverges. Therefore, since B_2 takes very large negative and positive values, we choose to present the rescaled quantity $\tilde{B}_2 = B_2(1 + |B_2|)/|B_2|$ on a logarithmic scale in figure 8 for sphere charge $Z = 40$ (a) and $Z = 100$ (b). The solid lines are obtained by full optimization of the effective Hamiltonian (4) and the broken lines show the results from constrained optimization. As expected, the unconstrained optimization always gives a lower value for B_2. The pronounced difference between the two curves in figure 8(a) is caused by PE bridging, which is quite prominent for $Z = 40$ (see figure 6(a)) because here the PE–sphere binding energy is smaller. The main trend is that B_2 has a minimum for intermediate salt concentrations, consistent with the general experimental trends [8]. Theoretically, it is worth mentioning that this high negative value of the second virial coefficient is not due to the bridging phenomena, since constrained optimization also gives a negative second virial coefficient, but it is due to the correlations of negative and positive charges on opposite complexes. Nonetheless, bridging also gives a highly negative B_2 when the effect of these correlations fades, as seen in figure 8(a). Here the minimum value for B_2, for both values of Z, occurs at $\kappa^{-1} \approx 1$ nm, which is of the order of the charge modulation on the surface of the complex. This also corresponds to the salt concentration at which a minimal sphere charge is needed to obtain a wrapped state (figure 4). In experiments also the minimum of the second virial coefficient occurs at about this salt concentration, although the value of B_2 is smaller. Within our model, smaller values for B_2 may be recovered by taking a smaller sphere charge $10 < Z < 20$.

4. Small-amplitude fluctuations

As mentioned in previous sections, thermal fluctuations are expected to be relatively unimportant for chain lengths that are short compared to the persistence length, allowing for a ground-state analysis in this regime. In fact, thermal fluctuations of the chains become important when the thermodynamics of the complexation process between PE chains and oppositely charged spheres are considered in solution, i.e. when one tries to describe the dissociation/association equilibrium. In this case, one has to account for the conformational entropy of the chains since it enters the law of mass action governing this equilibrium. The conformational entropy may be calculated from a normal-mode analysis of the chain fluctuations around the ground-state configuration on the charged sphere. In this section, we briefly discuss small-amplitude fluctuations (excited states) of the PE chain in a single complex, which generalizes the preceding ground-state analysis. The spectrum of chain fluctuations in different phases and the chain adsorption process will be discussed in detail elsewhere [56].

Let us assume that the ground-state configuration of the chain is given by a set of parameters represented by the vector $\mathbf{X}_0$, which in our model contains the polar and azimuthal angels of subunits of the discretized chain (figure 1). For small fluctuations around the ground state, the effective Hamiltonian of the complex (specified by the state vector $\mathbf{X} = \{x_n\}$) may be expanded around its minimum as

$$\beta\mathcal{F}(\mathbf{X}) \approx \beta\mathcal{F}_0 + \tfrac{1}{2}(\mathbf{X} - \mathbf{X}_0)^{\mathrm{t}}\mathbf{H}^{(2)}(\mathbf{X} - \mathbf{X}_0). \tag{8}$$

Here $\mathcal{F}_0 = \mathcal{F}(\mathbf{X}_0)$ is the energy of the optimal ground-state conformation and the superscript t denotes the transpose of the state vector. $\mathbf{H}^{(2)}$ is the Hessian matrix associated with the effective Hamiltonian, which is defined as

$$H^{(2)}_{nm} = \left(\frac{\beta\partial^2\mathcal{F}}{\partial x_n \partial x_m}\right)_{\mathbf{X}=\mathbf{X}_0}. \tag{9}$$

It characterizes the spectrum of chain excitations within the harmonic (or Gaussian) approximation. The normal modes of chain fluctuations in a complex are obtained by diagonalizing the Hessian matrix using the equation $\mathbf{H}^{(2)}\mathbf{A} = \mathbf{A}\mathbf{\Lambda}$, which is solved numerically for the matrix of eigenmodes, $\mathbf{A}$, and the diagonal matrix of eigenvalues, $\mathbf{\Lambda}$. The matrix elements of $\mathbf{\Lambda}$ are $\Lambda_{nm} = \lambda_n\delta_{nm}$ with λ_n being the eigenvalue associated with the nth normal mode and δ_{nm} being the Kronecker delta (where $n, m = 1, \ldots, 2N$ with $N = 250$ chosen as the optimal discretization degree).

In figure 9, we show in (a) the ground state and in (b) and (c) the second and the sixth excited states of the complex, respectively. The parameter values chosen are $Z = 40$ and $\kappa = 0$ such that the ground state corresponds to the fully symmetric phase IV (see section 2). As seen, the ground state's mirror symmetry is broken in the second excited state (figure 9(b)) and the twofold rotational symmetry is broken in the sixth excited state (figure 9(c)). The latter eigenmode can be viewed as a translational motion of the bound sphere along the PE chain. The spectrum of chain fluctuations (figure 9(d)) shows a behaviour close to that of an isolated PE chain at low mode numbers [56], since the ground state of the chain configuration has a shape close to a straight line. For higher-order modes, the chain exhibits fluctuations normal to the sphere surface, which are energetically quite costly and thus lead to the rapid increase of the eigenvalues for large n.

To obtain the full free energies of the various complex phases one has to sum over the entropic contributions of each eigenmode, which can be easily done once one knows the corresponding eigenvalues. The eigenvalues and entropic contributions are different in different complex phases. For example, the excitations around the ground state in phase III are less costly as compared to excitations in other phases, since the chain has a longer dangling

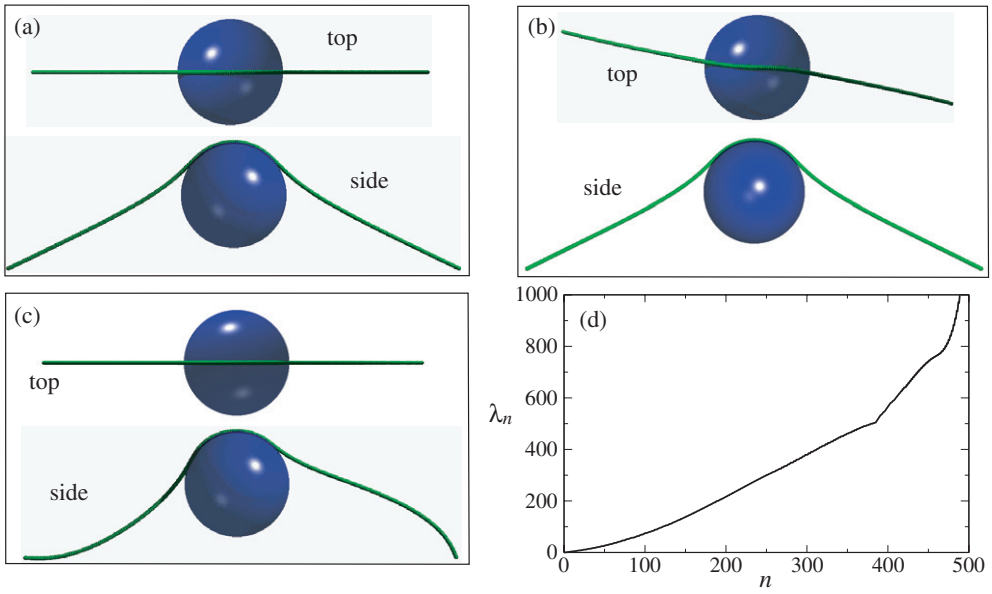

Figure 9. Normal modes and the spectrum of the chain fluctuations around the ground state with the symmetry class IV shown in (a) from top and side views (for $Z = 40$ and $\kappa = 0$). In (b) and (c), we show the second and the sixth excited states around this ground state; (b) shows a breaking of the mirror symmetry, and (c) shows a breaking of the twofold rotational symmetry. In (d) we show the spectrum of the chain fluctuations (eigenvalues, λ_n, as a function of the mode number n).

tail in this phase. Therefore, fluctuations in this phase contribute a higher entropy and the transition lines are shifted slightly [56].

5. Conclusion

In this paper we review the complexation of a semiflexible polyelectrolyte chain with an oppositely charged macroion, using parameters appropriate for the biologically relevant DNA–histone system. Electrostatic interactions are treated on the linear Debye–Hückel level. In the first part, we discuss the effect of salt concentration and effective sphere charge on the conformation of PE chains. Our results indicate that for sphere charges Z larger than a threshold $Z_* \approx 12$ we have four different configurational phases characterized by separately broken symmetries of the chain configuration on the sphere. For $Z < Z_*$, for all salt concentrations, the configuration exhibits the unwrapped state. Interestingly, the ionic strength needed to obtain a fully wrapped chain at the minimal sphere charge $Z_* = 12$ coincides with physiological salt conditions (monovalent salt concentration of 100 mM). The phase diagram indicates two regimes of wrapping–dewrapping transition at very low and very high salt concentrations. The high-salt dewrapping transition is due to complete screening of the electrostatic interactions and is driven by the bending rigidity of the chain. The low-salt dewrapping transition occurs at a value of screening length κ^{-1}, which is of the order of the sphere diameter. In this regime, the dewrapping transition is triggered by the electrostatic self-energy of the chain. The results are in agreement with experimental findings concerning the stability of the nucleosomal core particles with variation of salt concentration [21].

In the second part we investigate the interaction between two complexes. We study the configurational changes of two complexes at small separations by classifying them into

symmetric and asymmetric changes. The chain configurations are similar (symmetric) at large distances and dissimilar (asymmetric) at distances of the order of the screening length. The asymmetric phase can exhibit a whole spectrum of conformations, ranging from slight orientational changes of chains to a bridge formation between the two complexes. Typically, this asymmetric phase yields an attractive force between the two spheres, even in cases where the energy at contact is not lower than that at infinite separation due to the presence of an energy barrier at intermediate sphere separations. The interaction energies are used to calculate the second virial coefficient, which has a minimum at salt concentrations corresponding to the physiological condition (and for certain sphere charges can even become negative). This salt concentration indicates a screening length which is of the order of the wavelength of charge modulation on the complex, thus allowing a charge correlation which leads to a very strong attraction. This result is also in qualitative agreement with experimental findings [8]. It should also be relevant to mixtures of spheres and PEs as long as the concentrations are not too different. The concentrations also should not be too low, otherwise the complexes will fall apart.

Chain conformational fluctuations, which become important when one tries to determine the association/dissociation equilibrium, can for stiff chains be included via a normal-mode analysis, as shown in section 4. Here one determines the eigenmodes of the complex via diagonalization of the Hessian describing the chain fluctuations. The corresponding eigenvalue spectrum can be used to calculate the entropic gain due to chain fluctuations on the Gaussian level. The entropy loss that chains suffer as they bind to spheres determines the chemical association/dissociation equilibrium in a decisive way [56].

Acknowledgments

The authors acknowledge funds from the DFG German–French Network. Useful discussions with S Mangenot, A Naji and H Schiessel are also gratefully acknowledged.

References

[1] Dubin P L, Curran M E and Hua J 1990 *Langmuir* **6** 707
[2] McQuigg D W, Kaplan J I and Dubin P L 1992 *J. Phys. Chem.* **96** 1973
[3] Haronska P, Vilgis T A, Grottenmüller R and Schmidt M 1998 *Macromol. Theor. Simul.* **7** 241
[4] Gittins D I and Caruson F 2000 *Adv. Mater.* **12** 1947
[5] Gittins D I and Caruson F 2001 *J. Phys. Chem.* B **105** 6846
[6] Zhang H *et al* 1999 *J. Phys. Chem.* B **103** 2347
[7] Rouzina I and Bloomfield V A 1996 *J. Phys. Chem.* **100** 9977
[8] Mangenot S, Leforestier A, Vachette P, Durant D and Livolant F 2002 *Biophys. J.* **82** 345
[9] Mangenot S, Raspaud E, Tribet C, Belloni L and Livolant F 2002 *Eur. Phys. J.* E **7** 221
[10] Grosberg A Yu, Nguyen T T and Shklovskii B I 2002 *Rev. Mod. Phys.* **74** 329
[11] Sukhorukov G B *et al* 1998 *Polym. Adv. Technol.* **9** 759
[12] Caruso F, Caruso R and Möhwald H 1998 *Science* **282** 1111
[13] McGhee J D and Felsenfeld G 1980 *Annu. Rev. Biochem.* **49** 1115
[14] Kornberg R D and Klug A 1981 *Sci. Am.* **244** 48
[15] Widom J 1989 *Annu. Rev. Biophys. Biophys. Chem.* **18** 365
[16] Felsenfeld G 1992 *Nature* **355** 219
[17] van Holde K 1993 *Nature* **362** 111
[18] Felsenfeld G 1996 *Cell* **86** 13
[19] Luger K and Richmond T J 1998 *Curr. Opin. Struct. Biol.* **8** 33
[20] Stryer L 1995 *Biochemistry* (New York: Freeman)
[21] Yager T D, McMurray C T and van Holde K E 1989 *Biochemistry* **28** 2271
[22] Schiessel H 2003 *J. Phys.: Condens. Matter* **15** R699

[23] Harrington R E 1982 *Biochemistry* **21** 1177
[24] Uberbacher E C, Ramakrishnan V, Olins D E and Bunick G J 1983 *Biochemistry* **22** 4916
[25] Libertini L J and Small E W 1987 *Nucleic Acids Res.* **15** 6655
[26] Cui Y and Bustamente C 2000 *Proc. Natl Acad. Sci. USA* **97** 127
[27] Bennink M L *et al* 2001 *Nat. Struct. Biol.* **8** 606
[28] Marko J F and Siggia E D 1997 *Biophys. J.* **73** 2173
[29] von Goeler F and Muthukumar M 1994 *J. Chem. Phys.* **100** 7796
[30] Gurovitch E and Sens P 1999 *Phys. Rev. Lett.* **82** 339
[31] Golestanian R 1999 *Phys. Rev. Lett.* **83** 2473
[32] Marky N L and Manning G S 1991 *Biopolymers* **31** 1543
[33] Marky N L and Manning G S 1995 *J. Mol. Biol.* **254** 50
[34] Netz R R and Joanny J-F 1999 *Macromolecules* **32** 9026
[35] Schiessel H, Rudnick J, Bruinsma R F and Gelbart W M 2000 *Europhys. Lett.* **51** 237
[36] Mateescu E M, Jeppesen C and Pincus F 1999 *Europhys. Lett.* **46** 493
[37] Nguyen T T and Shklovskii B I 2001 *Physica* A **293** 324
[38] Nguyen T T and Shklovskii B I 2001 *J. Chem. Phys.* **114** 5905
[39] Schiessel H, Bruinsma R F and Gelbart W M 2001 *J. Chem. Phys.* **115** 7245
[40] Podgornik R and Jönsson B 1993 *Europhys. Lett.* **24** 501
[41] Podgornik R, Åkesson T and Jönsson B 1995 *J. Chem. Phys.* **102** 9423
[42] Podgornik R 2004 *J. Polym. Sci.* B **42** 3539
[43] Dzubiella J, Moreira A G and Pincus P 2003 *Macromolecules* **36** 1741
[44] Skepö M and Linse P 2003 *Macromolecules* **36** 508
[45] Stoll S and Chodanowski P 2002 *Macromolecules* **35** 9556
[46] Jonsson M and Linse P 2001 *J. Chem. Phys.* **115** 10975
[47] Wallin T and Linse P 1998 *J. Chem. Phys.* **109** 5089
[48] Netz R R and Joanny J-F 1999 *Macromolecules* **32** 9013
[49] Park S Y, Bruinsma R F and Gelbart W M 1999 *Europhys. Lett.* **46** 454
[50] Kunze K K and Netz R R 2002 *Europhys. Lett.* **58** 299
[51] Manning G S 1969 *J. Chem. Phys.* **51** 924
[52] Kunze K K and Netz R R 2000 *Phys. Rev. Lett.* **85** 4389
[53] Kunze K K and Netz R R 2002 *Phys. Rev.* E **66** 11918
[54] Israelachvili J 1991 *Intermolecular and Surface Forces* (London: Academic)
[55] Boroudjerdi H and Netz R R 2003 *Europhys. Lett.* **64** 413
[56] Boroudjerdi H and Netz R R 2005 at press